Underground Microseismic Monitoring of Pillar Systems to Evaluate Mechanism of Failure

A.M. Milev, M.W. Hildyard, L.M. Linzer, S.M. Spottiswoode CSIR Mining Technology, South Africa

Portable underground monitoring systems equipped with uniaxial and triaxial geophones were installed at two underground sites. The Microseismicity recorded at these sites was analysed in terms of spatial distribution of seismic events, peak particle velocities supported by numerical modelling of the wave-field around the pillar, as well as the source mechanism of seismic events.

A novel method for studying in situ pillar behaviour was developed and helped identify the mechanism of failure. Numerical models were created to simulate the wave propagation for possible failure mechanisms. The synthetic seismograms were compared with the observed seismograms in an attempt to find the greatest similarity. The moment tensor was obtained from the weighting coefficients used in the correlation. This methodology differs from the traditional inversion approach, and takes into account a far more complex geometry and the influence of this geometry on the waveforms.

Footwall slip along the narrow side of the pillar was found to be the probable mechanism for failure at both sites. Shear fractures of the pillar were also identified in support of this solution. The pillar fracturing was found to occur during and shortly after blasting, while the pillar was being cut.

1 INTRODUCTION

Most of the mining in the Bushveld Complex, South Africa, takes place at depths of less than 1500 m below the surface. All mining at these depths relies on various types of pillars to provide panel- as well as regional stability. 'Crush' and 'Yield' pillars are used extensively for in-stope support (Ozbay and Roberts, 1988).

In the former, pillar edge slabbing and internal conjugate shear fracturing have been noted as the failure mechanisms. Ideally 'Crush' pillars should fracture significantly as they are cut. However, to what extent this occurs under different mining conditions is not known. The yield mechanism of the second type of pillar is also unclear.

The pillar failure mechanism is known to be related to the following factors:

- the mining method and amount of mining;
- the ambient stress and the effect of various k-ratios;
- pillar width to length and height ratios;
- geological structures and type of host rock;
- the fracture formation around the hangingwall and footwall contacts;
- foundation failure;
- the magnitude of dynamic loading during the interaction with the seismic waves propagating through the excavations;
- strength variation within the reef.

These factors may vary significantly in different geotechnical areas. Most of the pillar failure models are associated with Microseismicity occurring before and during the failure. Detailed study of this seismic activity should indicate the state of stability of pillar systems.

In this study, the seismic data recorded underground by close-in Microseismic networks installed around different pillar systems is analysed; in particular, spatial distribution of the seismic events, peak particle velocities (PPVs), waveform analyses supported by numerical modelling of the wave-field around pillar failure, as well as the source mechanism.

2 UNDERGROUND MONITORING OF MICROSEISMICITY IN THE VICINITY OF PILLARS

Portable underground monitoring systems, the Impulse and Ground Motion Monitor, developed by CSIR Mining Technology, equipped with uniaxial and triaxial geophones were installed in site-specific configurations. Modifications such as increasing the sampling rate and expanding the frequency range towards the higher frequencies were made to increase the quality of seismograms of the Microseismic events associated with dynamic pillar behaviour. Two underground sites located in two different platinum mines, Amandelbult and Impala, were monitored.

2.1 Amandelbult Platinum Mine

Following the discussion with rock mechanics personnel at Amandelbult Mine (Akermann, 2003), a site at Shaft #1, 13–33, panel 1 West was instrumented. The recording configuration comprised one triaxial and seven uniaxial geophones. Figure 1 illustrates the mining layout and position of the geophones.

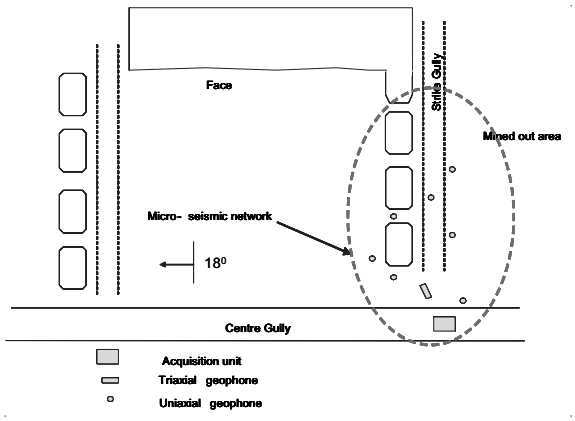

FIG. 1 Underground monitoring system installed at Amandelbult, Shaft #1, site 13-33, 1 W

During the monitoring period, 1026 seismic events were recorded. Most of the events were blasts. Clear separation of the blasting sequences was found for the entire data set. Most of the induced seismicity followed shortly after the blasting sequences.

2.2 Impala Platinum Mine

Following the discussion with rock mechanics personnel at Impala Mine (Scheepers, 2003; Miovsky, 2003), the site at Shaft #10, Level 17, 74 A was selected for monitoring. A recording configuration comprising one triaxial and five uniaxial geophones was installed. Figure 2 illustrates the mining layout and position of the geophones.

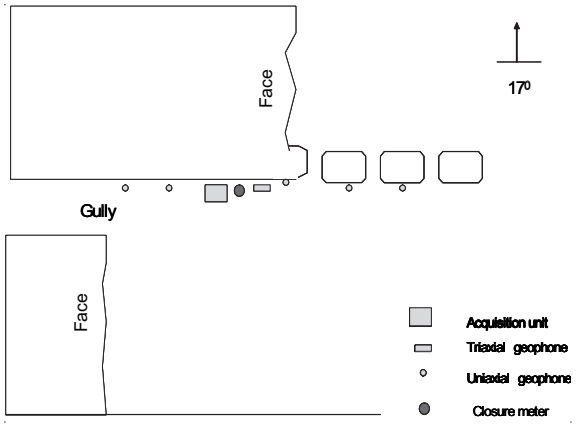

FIG. 2 Underground monitoring system installed at Impala, Shaft #10, site 17/74 A

During the monitoring period, 1068 seismic events were recorded. Two modes of seismic event distribution were identified. The first mode shows clear separation of the blasting sequences, similar to the pattern found for the Amandelbult data, and the second mode shows higher dispersion of the seismic events. The dispersion in the second mode was due to interruption in the production cycle at this site during the second part of the monitoring period.

A high degree of waveform similarity was found between the blasting seismic events and crush-type events associated with the pillar. An additional procedure, described below, was applied to separate the blasting events from mining-induced seismic events associated with the pillar failure.

2.3 Identification of Pillar-Associated Seismic Events

One of the important steps in this study was the identification of pillar-associated seismic events. This involved separating blasts from seismic events and distinguishing between face- and pillar seismic events. The first attempt to separate blasting and seismic events was carried out by cross-correlating the PPVs recorded at each channel and the time differences between two consecutive events. As most of the events were blasts with more or less similar time sequences, seismic events with low cross-correlation and greater time differences were selected as prospective seismic events.

Further processing of these events was done by visual comparison of the waveforms. All waveforms however, showed a high degree of similarity. Two factors contributed to this.

- 'Crush' pillars are designed to fracture when they are cut before they have formed their residual strength (Ozbay and Roberts, 1988). This process is associated with most of the pillar seismic events and occurs directly after the blasting time.
- Waveforms generated by the crush-type mechanism associated with the pillar punching are expected to have a blasting-type pattern.

An additional procedure based on temporal and spatial migration of seismic events was applied in the final separation. In this procedure, the level of PPVs generated by blasts and induced seismic events was taken into account. AURA, the seismic waveform processing and analysis program written by CSIR Mining Technology, was used to locate the seismic events and to calculate additional seismic information.

The first criterion used for the separation of blasts and seismic events was the time difference between two consecutive events and is called the 'inter-event time difference'. This difference is plotted in Figure 3 as a function in time.

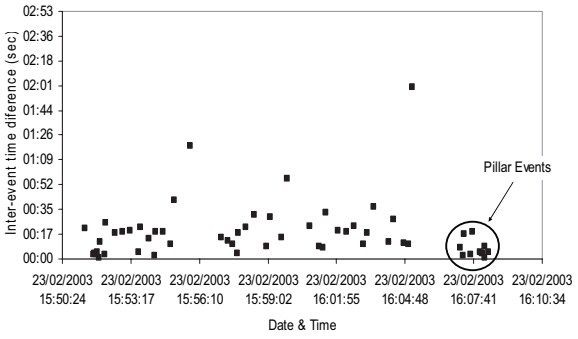

FIG. 3 Inter-event time difference

A clear gap between the blasting sequence and pillar-associated seismic events located towards the end of the blasting time can be seen in Figure 3. This gap is used as a separator between blast and seismic events. The time gap, however, was not very well pronounced for all blasting-event sequences that made up the data.

The second criterion used to separate blasts from induced seismic events was the spatial migration pattern of the events. The blasts are expected to migrate along the face towards the pillar as blasting progresses, and then be followed by the cluster of pillar seismic events. The observed spatial migration pattern progressed as expected, and the cluster of pillar seismic events was clearly separated from the blasting events (Figure 4).

The Peak Particle Velocity (PPV) is a widely used parameter in the mining industry for characterising the dynamic behaviour of excavations. A number of studies carried out in gold mines have shown strong variations of the PPVs with respect to the distance of the source from the pillar (Milev at al., 1999). The third criterion was based on the PPVs generated from the blast and seismic events (Figure 5).

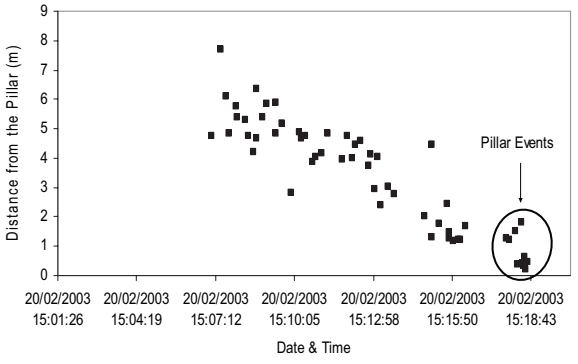

FIG. 4 Spatial migration of events from the face towards the pillar

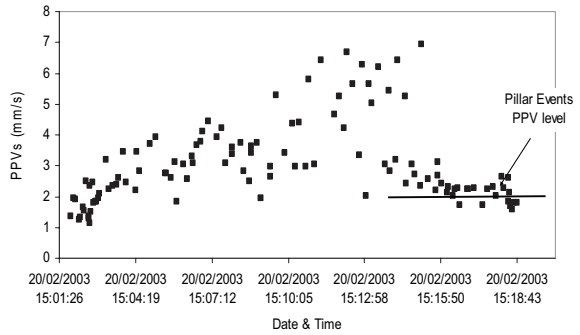

FIG. 5 PPVs recorded for both blasts and induced seismic events

It can be seen from Figure 5 that there is an increase in the PPVs while the blasts are propagated from the bottom of the panel towards the pillar, where the maximum of PPV is reached at the last blast. The events that occur after this point have lower PPVs and are associated with the pillar.

As a supplementary criterion for separation, the actual number of blasts per metre was used to calculate the expected number of blasts in the blasting-event sequence and was compared to the total number of events.

3 NUMERICAL MODELLING USING "WAVE" TO ANALYSE THE WAVE FIELD ASSOCIATED WITH PILLAR FAILURE

3.1 The WAVE Model

Models were created to simulate the wave propagation for some possible failure mechanisms. It is hypothesised that the source mechanisms are similar if the synthetic waveforms and the measured waveforms have common characteristics. The purpose of modelling therefore is to produce synthetic waveforms for these different source mechanisms, in order that they can be compared to the measured data. This hypothesis was tested for two characteristic models expected during the pillar failure.

The above methodology differs from a traditional inversion approach, where a moment tensor is inverted from waveforms measured at a number of different positions (Andersen and Spottiswoode, 2001). Typically, however, these inversions assume a very simple homogeneous elastic model and do not take account of the mining-free surfaces. The modelling readily takes account of a far more complex geometry, and the influence of this geometry on the waveforms was shown to be dominant. The trade-off is that a mathematical inversion is not easily achieved, and hence the analysis involves visual comparison of the simulated and measured waveforms.

The program WAVE (Cundall, 1992; Hildyard et al., 1995) was used in this analysis. A detailed description of its theory and applications can be found in Hildyard (2001) and Hildyard and Young (2002). WAVE has been applied extensively in a number of applications where modelling wave interaction with an excavation was required. Simulations of an excavation geometry and fractured material were found to produce waveforms consistent with those measured, and comparisons with the measured waveforms allowed conclusions to be reached on fracturing in the material. The work has been applied in both mining and nuclear waste storage problems, using models with different degrees and types of fracturing to help interpret the fracturing in measured waveforms. The application in this study is similar – the production of waveforms for different source mechanisms, rather than different types of fracturing, to help determine the failure mechanism.

3.2 Model Geometry and Strategy

The initial investigations and the evolution of the methodology were based on the Amandelbult site, with events from the first pillar. Four positions were investigated for a source aligned with each of the pillar faces. Modelled events were centred either in the footwall, hangingwall or reef to help identify the type of mechanism. This resulted in 12 types of mechanism based on location. Two types of failure were focused on shear slip parallel to a pillar face (assumed to represent 'punching'), and a reduction of vertical stress (assumed to represent 'crushing').

The mining geometry was modelled, assuming an elastic rockmass with P- and S- wave-velocities of 5740 m/s and 3514 m/s respectively. The modelled sources had an area of approximately 2 m^2, and were initiated at 10 ms, and their mid-point located 0.5 m into either the hangingwall or footwall, or were mid-seam. Waveforms were collected for both the uniaxial and triaxial geophone positions, although only the triaxial waveforms were used in the comparisons. The triaxial geophone was installed on the hangingwall surface.

Major changes were made to the initial model. The modelling analysis evolved in the following manner:

- Initial models tested finite-sized sources with particular mechanisms for slip or vertical stress drop.
- More varied source mechanisms were found to be necessary. Rather than model each mechanism separately, waveforms were obtained for point source models for each of the six basic source components (xx, yy, zz, xy, yz, zx) and for each source location. Any source mechanism for a location can be constructed from linear combinations of the basic components from that location. Given the 12 locations, 72 models were required.
- Initial models used a zero-width seam and stope. A model with a finite-width seam was developed and shown to be important for this analysis, given the geometry and source-size considerations.
- The final methodology is to propose event mechanisms, then construct these as linear combinations of the basic models. These are then compared with measured waveforms in order to evaluate whether there is evidence for the chosen mechanism.
- The mining geometry, position in the pillar, and event location in footwall, hangingwall or reef were all found to have significant effects on the waveforms, even though the location difference is only of the order of metres.

3.3 Initial Models – Finite-Sized Source, Fixed Mechanism, Thin Seam

Initial models tested finite-sized sources with particular mechanisms of slip and vertical stress drop. Six punching-type events were modelled: four positions in the footwall, at each face of the pillar, and two positions in the hangingwall, at the shortest and longest faces of the pillar. These were modelled as vertical shear slip events with different senses of shear depending on the likely stress drop for that location. Two crush-type events were also modelled as a drop in normal stress over a region in the pillar. An event that was located in the first pillar was selected for comparison with these test models.

The events were given a finite size (rather than a point source being used). Initially, it was assumed that only small pillar events would be observed, and a size of 0.5 m x 0.3 m with a 10 MPa stress drop was used. This was later adjusted

to 1.3 m x 1.3 m with the same stress drop. The larger source size is more consistent than the smaller source is with the pulse widths observed in the data.

The spectral analysis of seismic events located at the nearest face of the pillar shows corner frequencies of about 1300 Hz. This corresponds to a meter source radius (+/- 2 m diameter) from the Brune model.

A smaller source size is possible, but only if a high stress drop occurs far more slowly than is normal in fault models - viz. much more slowly than the shear wave velocity.

The waveform comparisons, however, showed no obvious mechanism – none of the chosen idealised mechanisms matched sufficiently in all components to suggest it was the likely mechanism. This motivated two alterations to the model; the first was to examine whether the thickness of the reef would influence results, and the second was to model the six basic source components (xx, yy, zz, xy, yz, zx) for each source location. This provides greater flexibility by allowing any source mechanism to be constructed from linear combinations of these basic components, rather than modelling each source mechanism individually. Given the 12 locations, 72 models were required. Each component was modelled as a point source, but the rise-time of the source was chosen to give pulse widths similar to the larger (~1.3 m x 1.3 m) source.

3.4 Importance of Seam Thickness

In many mining models applied to tabular seams, the thickness of the seam is neglected and the stope is modelled as a zero-thickness slit. However, for this study, the pillar is of a similar size to the seam thickness and events may be of similar size or much smaller. As a result, the seam thickness is significant relative to the wavelengths of interest. A thick seam model was therefore developed. The seismograms from the thin seam model were found to be significantly different from the seismograms from the thick seam model.

3.5 Vertical Position of Event – Hangingwall, Footwall or Reef?

The location of the source in the hangingwall, footwall or reef was found to make a significant difference to the seismograms and radiation patterns. Figure 6 illustrates the synthetic seismograms calculated at the nearest face of the pillar at the hangingwall and the footwall. These were computed and compared with the observed seismogram from the source located in the footwall.

Since the geophone was located in the hangingwall, a modelled event in the hangingwall had much higher amplitude than an event located in the footwall and reef, as a result of a more direct propagation path. The seismograms themselves differ considerably, with different components being dominant.

3.6 Modelling Guidelines

The following guidelines can be derived from this section:

- It is essential to model the true reef thickness, as this significantly affects the waveforms for this type of geometry and size of source.
- The event location - in terms of its position inside the pillar near a particular pillar face and whether in the footwall, hangingwall, or on-reef - has a significant effect on the waveforms.
- Models suggest that results could be improved simply by taking measurements at the same position for both the hangingwall and footwall. This should permit the identification of whether it is a footwall, hangingwall, or reef mechanism.

4 CALCULATION OF MOMENT TENSOR TO DESCRIBE THE SOURCE MECHANISM

4.1 Concept

The moment tensor can be computed using one of two approaches: by doing a forward modelling exercise, or by the process of inversion. In this study a forward modelling process was applied.

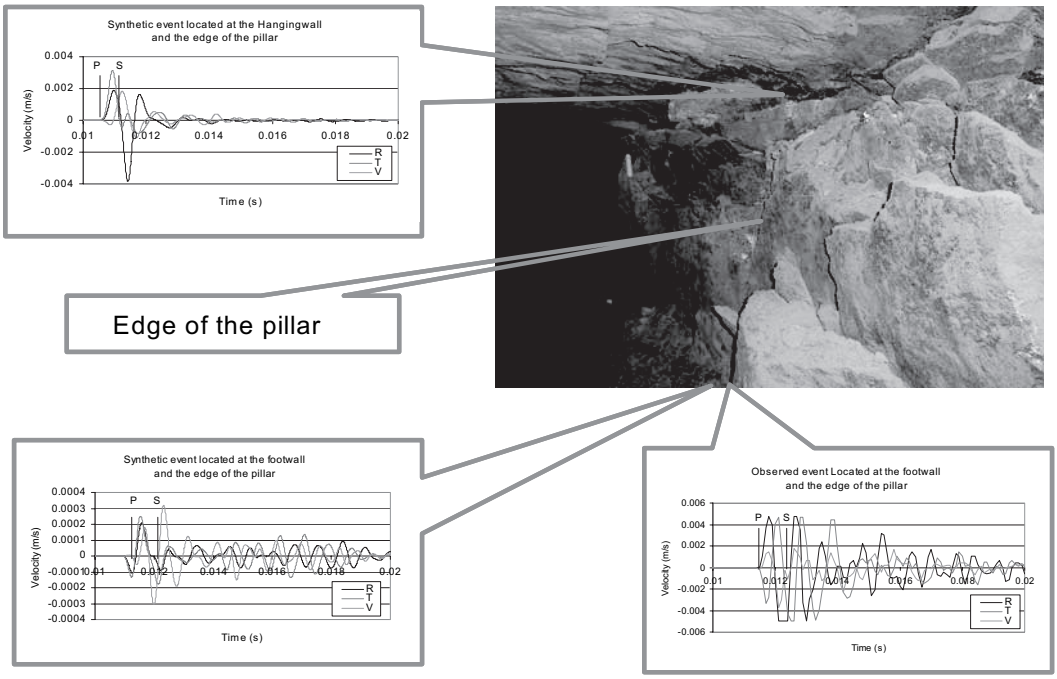

FIG. 6 Synthetic and observed seismograms for seismic events located in the edge of the pillar: R is the radial component; T is the tangential component, and V is the vertical component

Conceptually, the forward problem can be described by:

$$U = GM \quad [1]$$

where vector U (dimension n) consists of the data (e.g. sampled values of the integrated ground displacement); matrix G is an $n \times 6$ matrix and is composed of the Green's functions for each source-receiver combination; and M is the vector comprising the six independent moment tensor components. In the forward problem, the Green's matrix would be computed (for that particular network geometry, material properties and propagation effects), a likely moment tensor would be estimated, and the equation would be solved for vector U, the ground displacements. The calculated displacements would then be compared with the recorded displacements and, depending on the residuals, the moment tensor would be adjusted, and the process performed again (McGarr, 1992; Andersen, 2001).

A moment tensor can be used to describe a seismic source only if a number of important requirements are met. It is assumed that:

- the seismic source can be approximated by a point source, i.e. that the fault-plane dimensions are shorter than the wavelength of the seismic waves used in the inversion;
- the effect of the earth's structure on the seismic waves is modelled correctly. This involves calculating the Green's tensor, which describes the wave propagation between the seismic source and each receiver in the seismic network.

In relation to this second point, the Green's tensor may be thought of, simplistically, as comprising a 'geometrical component' and a 'path effect'. The former depends on the geometric relationship between the source and receiver, while the latter depends on the properties of the medium through which the seismic waves propagate.

If either of these requirements is not met, the computed moment tensor may contain a large non-double-couple component, even if the source mechanism is a double-couple. We will refer to this non-double-couple component as a 'false' component.

A further factor contributing to the presence of 'false' components in the moment tensor is the quality of the available data (Andersen, 2001). Waveforms recorded in the underground environment are subject to a number of types of systematic error, which in turn have an adverse effect on the moment tensor solutions. Factors such as raypath focusing and defocusing as a result of inhomogeneities in the rockmass; the degradation of the velocity model as a result of mining-induced fractures, joints and other discontinuities; low signal-to-noise ratios; and poor P- and S-wave picks all have a negative effect on the fidelity of the seismograms and can result in 'false' moment tensor components.

The forward modelling approach was taken in this study for two main reasons:

- The inversion problem was underdetermined (i.e. more 'unknowns' than data). The moment tensor (the unknown quantity) consists of six independent variables, whereas only a maximum of four independent data points were available for each recorded event.
- The pillar geometry had a pronounced effect on the raypath between the event sources and receivers. (This is demonstrated above in Section 3.) Complicated Green's functions would be needed to model such raypaths - otherwise the resultant moment tensors could contain false components. Unfortunately, the moment tensor inversion software currently available assumes simple, far-field Green's functions calculated using a straight raypath and is therefore not suited to this particular problem. The Green's functions appropriate to the pillar geometry can be calculated by numerical modelling codes, such as WAVE.

4.2 Methodology

The forward modelling process discussed above was applied to compute the mechanisms. This involved calculating 72 synthetic waveforms for each of the six basic moment tensor components for 12 source positions in the pillar.

Linear combinations of the synthetic seismograms for the six basic moment tensor sources were then compared with the recorded seismograms. To facilitate this comparison, the synthetic seismograms were rotated into the co-ordinate system of the geophones. The linear combinations of the tensor components were adjusted until there was a high degree of similarity between the polarity, amplitude, and frequency of the synthetic and recorded seismograms. The moment tensor resulting from this forward modelling process was then rotated into the geographical co-ordinate system using the following equation:

$$m_{\bar{i}\bar{j}} = \gamma_{\bar{i}k}\gamma_{\bar{j}l}m_{kl} \quad [2]$$

where m_{ij} is the ij^{th} element of the transformed matrix $\overline{M}$ and m_{kl} is the kl^{th} element of the original matrix (AND?) M and γ are the direction cosines between the rotated and unrotated axes. Summation over repeated indices applies.

A transformation is required to rotate the moment tensor M, from an "+x,+y,+z" system where +x = 18° W of N; +y = up and +z = 72° E of N into the required "+North, +East, +Down" system. Thereafter, the focal mechanisms were related to pillar geometry for each particular case. The results are described in the following section.

5 RESULTS AND DISCUSSION

5.1 Modelled Mechanisms and Application to Measured Waveforms

The initial model established that there were significant differences in modelled waveforms depending on whether the event was located in the footwall, hangingwall or reef, and on which of four pillar faces it occurred. Models for the six basic source components were simulated for each of these possible locations, from which any source mechanism could be constructed.

This section tests selected recordings from the Amandelbult and Impala sites against a range of possible theoretical mechanisms. Several likely failure mechanisms are proposed. Simulated waveforms were then constructed for each mechanism and each location, using linear combinations of the basic source components. Each mechanism was tested against the data, allowing some mechanisms to be eliminated, while others were consistent for certain locations in the pillar.

5.2 Selected Mechanisms

The mostly likely mechanisms of failure were considered to be shear in the hangingwall and footwall, or crushing or spalling in the reef. The following failure mechanisms were tested and are illustrated in Figure 7.

These mechanisms were implemented in WAVE, using the relative stress drops for each pillar position shown in Table 1. In all cases, the outwards and inwards slips were only slightly off the vertical in these mechanisms (around 10 degrees). The 'natural' sense of slip for the hangingwall or footwall is generally considered to be such that material

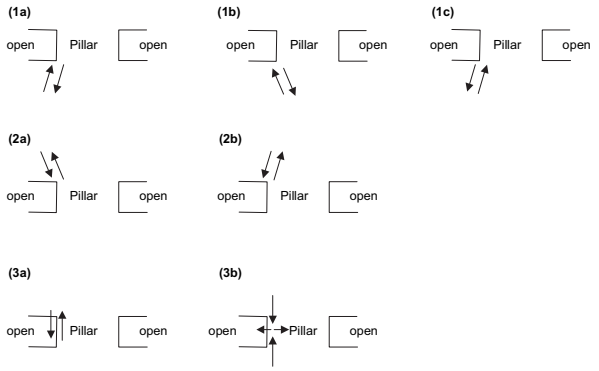

FIG. 7 Mechanisms tested in the simulations. Mechanisms at different locations along the pillar, compared with recordings

moves in towards the opening. These cases are identified as a 'natural' sense of slip. Evaluating the opposite sense of slip for a footwall event was also found to be useful.

TABLE 1 Relative values of stress drop (σ is in MPa) used in WAVE to implement the various source mechanisms at different pillar positions

Mechanism	Location 'a'	Location 'b'	Location 'c'	Location 'd'
F/W 1a	σ_{23}=-20; σ_{22}=-5; σ_{33}=+5;	σ_{23}=+20; σ_{22}=-5; σ_{33}=+5;	σ_{12}=+20; σ_{22}=-5; σ_{11}=+5;	σ_{12}=-20; σ_{22}=-5; σ_{11}=+5;
F/W 1b	σ_{23}=-20; σ_{22}=+5; σ_{33}=-5;	σ_{23}=+20; σ_{22}=+5; σ_{33}=-5;	σ_{12}=+20; σ_{22}=+5; σ_{11}=-5;	σ_{12}=-20; σ_{22}=+5; σ_{11}=-5;
F/W 1c	σ_{23}=+20; σ_{22}=+5; σ_{33}=-5;	σ_{23}=-20; σ_{22}=+5; σ_{33}=-5;	σ_{12}=-20; σ_{22}=+5; σ_{11}=-5;	σ_{12}=+20; σ_{22}=+5; σ_{11}=-5;
H/W 2a	σ_{23}=+20; σ_{22}=-5; σ_{33}=+5;	σ_{23}=-20; σ_{22}=-5; σ_{33}=+5;	σ_{12}=-20; σ_{22}=-5; σ_{11}=+5;	σ_{12}=+20; σ_{22}=-5; σ_{11}=+5;
H/W 2b	σ_{23}=+20; σ_{22}=+5; σ_{33}=-5;	σ_{23}=-20; σ_{22}=+5; σ_{33}=-5;	σ_{12}=-20; σ_{22}=+5; σ_{11}=-5;	σ_{12}=+20; σ_{22}=+5; σ_{11}=-5;
Reef 3a	σ_{23}=+20;	σ_{23}=-20;	σ_{12}=-20;	σ_{12}=+20;
Reef 3b	σ_{22}=+20; σ_{33}=-20;	σ_{22}=+20; σ_{33}=-20;	σ_{22}=+20; σ_{11}=-20;	σ_{22}=+20; σ_{11}=-20;

5.2.1 Footwall mechanisms

1a Outwards slip, with slip-sense such that motion is upwards into the open stope and downwards on the pillar side ('natural' sense of slip). Shear plane dipping away from the pillar.

1b Outwards slip, with slip-sense such that motion is upwards into the open stope and downwards on the pillar side ('Natural' sense of slip). Shear plane dipping into the pillar.

1c Outwards slip, with slip-sense such that motion is downwards on the stope side and upwards on the pillar side. This is the opposite sense of slip to that normally assumed.

5.2.2 Hangingwall mechanisms

2a Outwards slip, with slip-sense such that motion is downwards into the open stope and upwards on the pillar side ('natural' sense of slip). Shear plane dipping away from the pillar.

2b Outwards slip, with slip-sense such that motion is downwards into the open stope and upwards on the pillar side ('natural' sense of slip). Shear plane dipping into the pillar.

5.2.3 On-reef failure

3a Vertical slip, with slip-sense such that motion is downwards on the stope side.

3b Crushing or spalling such that convergence occurs and material moves towards the stope.

5.3 Amandelbult Site

A plan view of the model geometry, the geophone position, and the four source locations is shown in Figure 8.

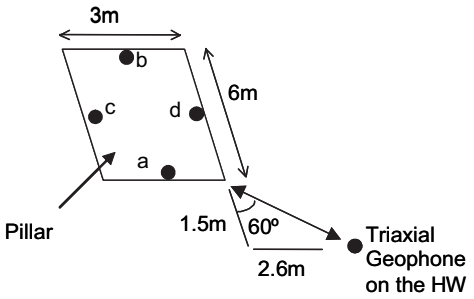

FIG. 8 Model geometry for Amandelbult site, showing source locations 'a', 'b', 'c' and 'd', relative to the position of the triaxial geophone

Two events were selected from the Amandelbult data - Event #57 and Event #129, located at the first pillar (Figure 1). Seismic analysis showed that Event #129 was located further from the geophone than Event #57, more likely corresponding to source positions 'b' or 'c', while Event #57 was located on the near face of the pillar at either positions 'a' or 'd'. The comparison between observed seismograms and the linear combinations of the synthetic seismograms for the six basic moment tensor sources were then carried out to estimate the source mechanism.

An example of synthetic and observed seismograms for Event #129 is shown in Figure 9.

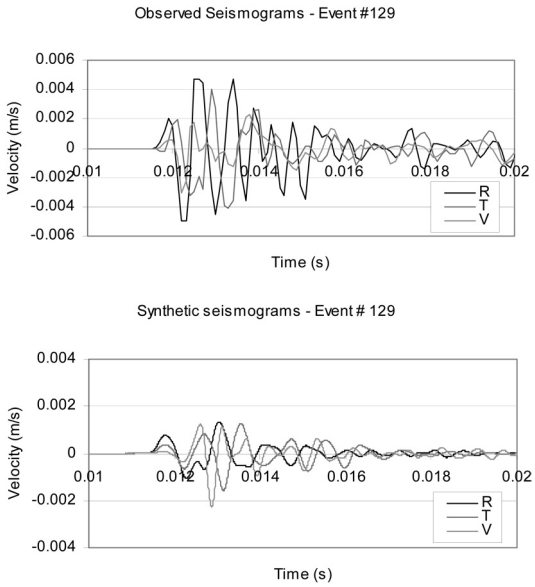

FIG. 9 Observed and synthetic seismograms at position b for Event #129 from the Amandelbult site: R is the radial component; T is the tangential component, and V is the vertical component

Maximum waveform similarity was found for the third footwall mechanism (1c, outwards slip), position 'b,' which indicates similar polarisation and consistency with the relative amplitude of the vertical velocity. The tangential velocity is relatively too high, and probably indicates a higher angle off the vertical.

The reef mechanism at position 'b' also indicates consistency and acceptable relative value for vertical velocity. Outwards in the reef at position 'b' is also a possible mechanism for Event #129.

The weighting coefficients used in correlation between observed seismograms and combined synthetic seismograms were used to calculate the nodal planes for both Event #57 and Event #129. Figure 10 shows the orientation of the nodal planes for these events.

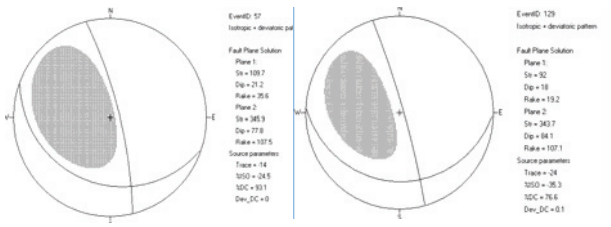

FIG. 10 Fault plane solution for Event 57 and Event 129, Amandelbult site

Both Events #57 and #129 are located at the short sides of the pillar (Event #57 at the closer side and Event #129 at the distant side) and they indicated similar mechanism. A nearly vertical slip type mechanism with plane oriented along the short side of the pillar was found. This indicates that pillar-punch and footwall-heave processes were likely to have taken place.

The moment tensor analysis in this work can be extended further to estimate the volumetric change during the pillar failure. The close relationship between the energy release through seismic failure and of stope closure (McGarr, 1976; Milev et al., 1995) is used to explain the overall stope behaviour during a seismic event generated during the process of pillar failure.

The relationship between the trace of the moment tensor (which is calculated from the diagonal elements) and the coseismic volume change can be written (McGarr, 1992) as:

$$\Delta V = tr(M_{ij})/(3\lambda + 2\mu) \qquad [3]$$

where, $tr(M_{ij})$ is moment tensor trace; λ and μ are Lame's elastic moduli.

In this study, the moment tensor trace was calculated from the modelled source as $tr(M_{ij})=6^7$ N–*m*. The values λ and μ were calculated by applying Hook's law to laboratory measurements of Young's modulus Y = 130 *GPa* and Poisson's ratio σ = 0.27 for pyroxenite rock samples (Sellers, 2004). The laboratory measurements of Y were then increased by 35% to compensate for the difference between static and seismically determined values (Ryder and Jager, 2002). Thereafter, we have $3\lambda + 2\mu = 2.71\times10^{11}$ *Pa*.

The moment of the each particular seismic event was estimated from the model source scaled using the amplitude ratio between observed and synthetic seismograms at the point of best similarity between them.

The volumetric change for Event #57 equals 2.95E-4 m^3 and that for Event #129 equals 2.6E-4 m^3. The small difference in the volumetric change between these events could be explained by their geometrical position, i.e. Event #57 is located at the outer side of the pillar, closer to more mined-out area and a footwall gully, while Event # 129 is located between two pillars closer to the solid ground. However, the difference is not significant and could be due to minor differences in strength of these seismic events.

It is also interesting to notice that the pillar failure happened immediately after blasting time or, in other words, during the formation of the pillar. This follows from the temporal analyses of the seismic events, where the pillar-associated events occurred at the end of the blasting time in all of the cases. Similar results were outlined by Ozbay et al. (1994).

5.4 Impala Site

The modelled geometry for the Impala site is shown in Figure 11.

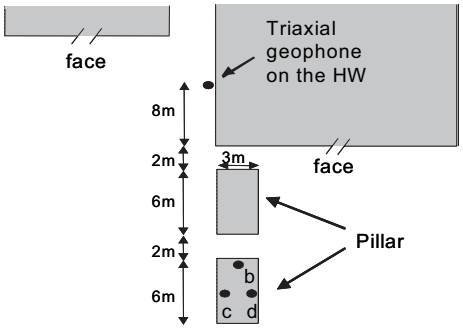

FIG. 11 Plan view of model geometry for Impala site, showing source locations 'b', 'c' and 'd', relative to the position of the triaxial geophone

An event that was clearly located on the second pillar was selected from the Impala data for further study.

The waveforms are shown in Figure 12. The modelled event was significantly further from the geophone than that from the Amandelbult data. Only positions 'b', 'c', 'd', were modelled, as position 'a' was excluded by the seismic analysis.

The first footwall slip mechanism has the correct polarities of first arrivals for source position 'b'. In addition, the radial component matches reasonably well, and is dominant as in the data. Outwards - near vertical slip mechanism '1c' in the footwall at position 'b' - is the corresponding mechanism for this seismogram.

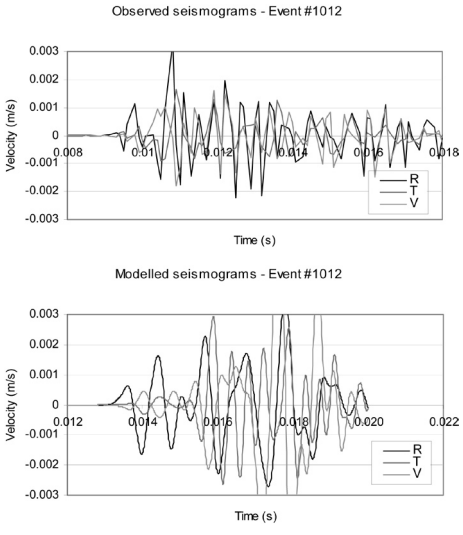

FIG. 12 Observed and synthetic seismograms at position 'b' for Event #1012 from the Impala site: R is the radial component; T is the tangential component, and V is the vertical component

6 CONCLUSIONS AND RECOMMENDATIONS

This study constitutes pioneering work in understanding the mechanisms of pillar failure, and has provided credible and useful results:

- A unique new method for studying in situ pillar behaviour has been developed.
- Footwall slip along the narrow side of the pillar was found as the probable mechanism for both sites. Shear fracturing of the pillar was also identified.
- The pillar fracturing occurred during and shortly after blasting, while the pillar was being cut.

In addition, two important lessons were learned in the course of this work:

- It is essential to model the true reef thickness as this significantly affects the waveforms for this type of geometry and size of source.
- The event location in terms of its position inside the pillar - near a particular pillar face, and whether in the footwall, hangingwall, or on-reef - has a significant effect on the waveforms.

Further work is therefore recommended to obtain a better understanding of pillar behaviour in platinum mines, with particular emphasis on the following:

- An increase in the location accuracy by using a denser 3-D seismic array, including geophones grouted in footwall and hangingwall boreholes. It would also be prudent to carry out active seismic velocity scans in the footwall, hangingwall, and reef
- Enhancement of the existing inversion method using heterogeneous Green's function estimated for platinum mining environment.

ACKNOWLEDGMENTS

This study was funded by PlatMine collaborative programme under Project PlatMine 1.4. The authors would like to express grateful acknowledgment to the rock engineering staff of the Amandelbult and Impala Mines for their assistance and cooperation.

REFERENCES

Akermann, K. (2003) Rock Mechanics Department, Amandelbult Platinum mine, personal communication, Northam, South Africa.

Andersen, L.M. (2001) A relative moment tensor inversion technique applied to seismicity induced by mining. PhD Thesis University of Witwatersrand, Johannesburg, South Africa.

Andersen, L.M. and Spottiswoode, S.M. (2001) A hybrid moment tensor inversion methodology. In Proceedings of the Rockbursts and Seismicity in Mines conference, Magaliesberg, South Africa.

AURA (2003) Software for routine and scientific processing of seismic data. CSIR Mining Technology, Johannesburg South Africa.

Cundall, P.A. (1992) Theoretical basis of the program WAVE. Unpublished internal report. COMRO (now CSIR Division of Mining Technology, South Africa), pp. 1-12.

Hildyard, M.W., Daehnke, A. and Cundall, P.A. (1995) WAVE: A computer program for investigating elastodynamic issues in mining. Proc. 35th U.S. Symp. on Rock Mech., June 1995, Balkema, pp. 519-524.

Hildyard, M.W. (2001) WAVE interaction with underground openings in fractured rock. PhD Thesis, University of Liverpool, Liverpool, UK, 252 p.

Hildyard, M.W. and Young, R.P. (2002) Modelling wave propagation around underground openings in fractured rock. Special Issue on Induced Seismicity, editors Trifu, Pure and Applied Geophysics, Vol. 159, pp. 247-276.

McGarr, A. (1976) Seismic moment and volume changes, J. Geophys. Res., 81, pp. 1487 - 1494.

McGarr, A. (1992) Moment tensors of ten Witwatersrand mine tremors. PAGEOPH, Vol 139, No. 3/4, pp. 781- 801.

Milev, A.M., Spottiswoode, S.M. and Noble, K.R. (1995) Mine Induced Seismicity at ERPM, Int. J. of Rock Mechanics and Mining Sci. & Geomech. Abstr., Vol. 32, pp. 629-632.

Milev, A.M., Spottiswoode, S.M. and Stewart, R.D. (1999) Dynamic response of the rock surrounding deep level mining excavations. Proc. 9th ISRM, G. Vonille & P. Berset (Editors), Paris'99: pp. 1109-1114.

Miovsky, P. (2003) Rock Mechanics Department, Impala Platinum mine, personal communication, Rustenburg, South Africa.

Ozbay, M.U. and Roberts, M.C.K. (1988) Yield pillars in stope support. Proc. of SANGORM Symposium Rock Mechanics in Africa, November 1988, Swaziland.

Ozbay, M. U., Ryder, J.A. and Jager, A.J. (1994) A literature and mine survey on the design of pillar systems in tabular hard rock mines. Final Project Report GAP 027/028. Pretoria: Department of Minerals and Energy.

Ryder, J.A. and Jager, A.J. (Editors) (2002) Rock mechanics for tabular hard rock mines, SIMRAC, p 489.

Scheepers, J. (2003) Rock Mechanics Department, Impala Platinum mine, personal communication, Rustenburg, South Africa.

Sellers, E. J. (2004) Personal communication, CSIR – Mining Technology, Auckland Park 2006, South Africa.